Simultaneous Calibration of Boresight and Lever Arm for Mobile LiDAR Systems on Hydrographic Platforms Using Synthetic and Real Data

Jordan McManus[1], Christian Larouche[2], Mohsen Hassanzadeh Shahraji[3]

[1] Department of Geomatics Sciences, Laval University, Quebec City, Canada - jordan.mcmanus.1@ulaval.ca
[2] Department of Geomatics Sciences, Laval University, Quebec City, Canada - christian.larouche@scg.ulaval.ca
[3] Quebec Geomatics Center, Chicoutimi, Canada - mohsen.shahraji@cgq.qc.ca

Keywords: LiDAR, Calibration, Boresight, Lever Arm Offsets, Synthetic Data, Spherical Targets.

Abstract

This work presents a robust calibration framework for marine LiDAR systems by leveraging spherical targets to jointly estimate boresight angles and lever arm offsets. The use of spheres provides a geometrically consistent and orientation-independent reference, enabling accurate calibration even in complex marine environments. To evaluate the proposed approach, a synthetic data generation algorithm was developed to simulate LiDAR scans over spherical targets, allowing controlled experiments across a wide range of sensor configurations. Furthermore, the calibration method was validated using real LiDAR data collected from a hydrographic survey vessel. Due to the calibration, the distance between the surveyed spherical centers and their estimated center positions from LiDAR point clouds is minimised to an RMS error of 0.036 m, which is within the range of the accuracy of the POS MV navigation system. We finally introduce a low cost in-house mobile LiDAR system integrating similar sensors in the ROS environment in order to address the challenges of obtaining LiDAR data in varying environmental conditions.

1. Introduction

The digital transformation of maritime platforms relies on the creation of high-fidelity digital twins, which move port management from static supervision to dynamic, data-driven orchestration (González-Cancelas et al., 2025). The foundation of this architecture lies the 3D data model, typically initialized through the integration of BIM and geospatial data captures of critical assets such as berths, cranes, and warehouses. To maintain the ”living” nature of a digital twin, regular data acquisition is required to reflect the as-built reality of infrastructure above sea level. Mounting Mobile LiDAR Systems (MLS) on marine vessels has emerged as a primary solution for this task, enabling high-speed continuous 3D mapping of quay walls and piers from the waterside—perspectives often inaccessible to land-based platforms. These vessel-based systems synchronize LiDAR scanners with GNSS and IMU sensors to provide a comprehensive, georeferenced point cloud of the terminal’s structural interface.

However, the utility of these 3D models for engineering-grade applications like structural health monitoring or automated logistics is entirely dependent on the robustness of system calibration. Robust calibration is essential to resolve the angular and spatial offsets between the LiDAR optical center and the inertial navigation system, as even marginal errors in sensor alignment are magnified over distance, leading to significant geometric distortions (Mendez, 2024). When properly calibrated, the resulting data provide the sub-centimeter accuracy necessary for ”scan-to-BIM” workflows. These high-integrity data allow port authorities to conduct precise change detection, verify as-built specifications against original designs, and populate digital twins with reliable spatial metadata that inform predictive maintenance and long-term infrastructure resilience.

The primary objective of this paper is to address the practical limitations of current calibration methodologies in restrictive maritime environments. Conventional calibration approaches (Shahraji and Larouche, 2022, Liu et al., 2022) typically assume that spatial (lever arm) offsets between the LiDAR scanner’s optical center and the INS center of gravity are precisely premeasured; however, such measurements are often unattainable when sensors are obscured by the vessel’s hull or complex mounting structures. Since it is impractical to remove vessels from the water for terrestrial measurements, we introduce a robust procedure utilizing spherical targets that enables the simultaneous estimation of all six degrees of freedom—comprising three boresight angles and three lever arm offsets—while the vessel remains in dynamic waters. The isotropic geometry of a sphere provides a consistent perspective from any viewing angle, facilitating more reliable centroid estimation regardless of the vessel’s relative position or motion. This method enables frequent calibration campaigns, ensuring a rigorous geometric foundation for accurate as-built models and port digital twins without the need for dry-docking.

2. Litterature Review

Accurate extrinsic calibration between LiDAR and IMU sensors is essential for high-precision mobile mapping systems. The calibration problem consists of estimating the rigid-body transformation (rotation and translation) between the LiDAR frame and the IMU frame, often referred to as the *boresight alignment*. Errors in this transformation directly propagate into georeferencing inaccuracies, especially in marine mobile LiDAR systems.

Several studies have proposed target-free approaches that rely on motion excitation and geometric constraints extracted from the environment. In (Mishra et al., 2021), the authors estimate the extrinsic parameters by exploiting motion-induced constraints without requiring pre-defined calibration targets. The method leverages the consistency between LiDAR-derived motion estimates and IMU measurements. Although effective in structured environments, such approaches depend heavily on sufficient motion excitation and environmental geometry richness.

https://doi.org/10.5194/isprs-archives-XLIX-B1-2026-307-2026

Similarly, (Glira et al., 2015) proposes an automatic calibration framework using geometric primitives such as planes and edges extracted from the environment. The calibration is achieved by minimizing the discrepancies between the features observed across multiple trajectories. Although the method removes the need for dedicated targets, it assumes stable and well-defined geometric features, which may not always be available in marine or unstructured environments.

(Zhu et al., 2022) focuses on the initialization problem in tightly coupled LiDAR–IMU systems. The work emphasizes the importance of proper motion excitation and observability of the system to reliably estimate extrinsic parameters. The study highlights that certain motion patterns are required to make the calibration parameters observable.

The issue of parameter observability is further addressed in (Lv et al., 2022). This work provides a theoretical analysis of the observability conditions of intrinsic and extrinsic parameters. It shows that insufficient excitation or poor geometric diversity can lead to degenerate solutions or biased parameter estimates. This theoretical insight is particularly relevant for marine applications, where motion may be constrained and environmental geometry limited.

Although target-free and self-calibration approaches reduce operational complexity, they exhibit several limitations in mobile LiDAR applications:

1. Limited geometric diversity in maritime environments (water surfaces, sparse vertical structures).
2. Reduced observability due to constrained motion dynamics.
3. Sensitivity to environmental noise and feature extraction instability.
4. Difficulty in validating calibration accuracy independently.

In such contexts, purely feature-based calibration methods may suffer from weak constraints, leading to suboptimal boresight angles estimation.

To address the limitations of target-free approaches, the use of pre-defined calibration targets provides strong geometric constraints and controlled observability conditions.

Spherical targets offer several advantages for boresight calibration:

- **Geometric Isotropy:** A sphere has uniform curvature in all directions, making its center estimation independent of sensor viewpoint and orientation.
- **Robust Center Estimation:** The center of a sphere can be estimated with high precision using least-squares fitting, even under partial occlusion.
- **Orientation Independence:** Unlike planar or edge features, spherical targets do not introduce directional bias in residual minimization.
- **Strong Rotational Constraints:** Multiple spheres distributed spatially provide well-conditioned constraints for estimating rotational misalignment.
- **Controlled Observability:** Pre-defined target placement allows the deliberate design of configurations that maximize parameter observability.
- **Validation Capability:** Residuals between measured and adjusted sphere centers provide a direct and interpretable quality metric.

In marine mobile LiDAR systems, where natural geometric features are often sparse or unstable, spherical targets provide a repeatable and geometry-rich calibration environment that reduces dependency on environmental structure and motion excitation, improving robustness and reliability of boresight estimation. Although the literature shows a shift from target-based to target-free calibration methods with increased automation and efficiency, theoretical observability analyses and practical limitations in structured and marine settings highlight the need for strong geometric constraints. In this context, spherical targets offer an operationally robust and geometrically optimal solution by providing controlled, isotropic, and high-precision spatial references that ensure reliable estimation of extrinsic parameters.

3. Methodology

Our calibration method is first developed and tested using synthetic data generated by a ray-tracing algorithm using a line-sphere intersection model and is subsequently validated using real scan data. Mobilizing a hydrographic team for marine surveying is a costly operation and the ability to generate synthetic data allows the reuse of previous survey trajectories to analyze calibration methods. The real data is acquired using a VLP-16 LiDAR scanner mounted on a hydrographic vessel and the synthetic data is modelled on this sensor's output format. The elevation angle is constant for each beam and ranges between -15°and 15°. The timings for the firing sequence for the VLP-16 are available in the product documentation and the sweeping angle has a configurable rate between 300 RPM and 1200 RPM. This configuration is used to interpolate the sweeping angle time series to the laser pulse firing sequence and to generate a unit launch vector for each pulse for both the synthetic data generation and the real data processing as represented by equation 1:

$$\mathbf{u}^{\ell} = \begin{bmatrix} \cos(\omega)\sin(\theta) \\ \cos(\omega)\cos(\theta) \\ \sin(\omega) \end{bmatrix} \tag{1}$$

where $\mathbf{u}^{\ell}$ = unit launch vector in LiDAR frame ℓ
θ = sweeping angle for laser pulse
ω = elevation angle for laser beam

This unit launch vector is first transformed into the inertial navigation system (INS) frame (i) using the boresight orientation matrix calculated from the boresight alignment angles. These angles are initially estimated and subsequently determined by the calibration algorithm. The unit launch vector can then be transformed into a local geodetic reference frame (LGF), using the platform orientation matrix calculated from the roll, pitch, and heading angles. These values are available in a smoothed best estimated trajectory (SBET), an output of the Applanix post-processing software suite Pospac. The unit launch vector is transformed according to equation 2:

$$\mathbf{u}^g = R_i^g(r,p,h)R_\ell^i(\alpha,\beta,\gamma)\mathbf{u}^\ell \tag{2}$$

where $\mathbf{u}^g$ = unit launch vector in LGF g
$\mathbf{u}^\ell$ = unit launch vector in LiDAR frame ℓ
$R_i^g(r,p,h)$ = platform orientation matrix
$R_\ell^i(\alpha,\beta,\gamma)$ = boresight orientation matrix
(r,p,h) = roll, pitch and heading angles
(α,β,γ) = boresight alignment angles

It is also necessary to determine the position of the scanner's optical center, $\mathbf{o}^g$, at the moment the laser pulse is fired as indicated in equation 3.

$$\mathbf{o}^g = \mathbf{P}^g + R_i^g(r,p,h)\mathbf{a}^i \tag{3}$$

where $\mathbf{o}^g$ = scanner's optical center in LGF g
$\mathbf{P}^g$ = platform position in LGF g
$\mathbf{a}^i$ = lever arm offset in INS frame i
$R_i^g(r,p,h)$ = platform orientation matrix
(r,p,h) = roll, pitch and heading angles

Other than noise and errors, the main difference is that for synthetic data, the range is determined mathematically while for real data it is one of the sensors' observations. The following section explains how to mathematically produce ranges for synthetic 3D points.

3.1 Synthetic data production

The main purpose of using synthetic data is to isolate the boresight angle errors and the lever arm offset errors from other sources of errors and noise. The trajectory of the platform and the position of the spherical targets used to create this synthetic data are considered as ground truth. For this experiment, we chose a trajectory from a previous survey as shown in Figure 1.

For the LiDAR data, we consider the elevation angle and the sweeping angle time series to be ground truth and the range data is geometrically generated by calculating the intersection between a line and a sphere (Eberly, 2001) in a local geodetic frame. This process is achieved by ray-tracing the unit launch vector for each laser pulse from the optical centre to the spherical target. In order to simplify the model, we ignore the speed of light and consider the ray-tracing to be an instantaneous process. The ray-traced distance d from the scanner's optical centre to the spherical target is given by equations 4 and 5 which is a quadratic equation where we keep the closest point since the beam does not go through the target. For most pulses, no intersection will be found since the launch vector does not point toward the spherical target causing the discriminant to be negative.

$$\nabla = [\mathbf{u}^g \cdot (\mathbf{o}^g - \mathbf{c}^g)]^2 - \left(\|\mathbf{o}^g - \mathbf{c}^g\|^2 - r^2\right), \tag{4}$$

$$d = -[\mathbf{u}^g \cdot (\mathbf{o}^g - \mathbf{c}^g)] \pm \sqrt{\nabla}, \tag{5}$$

where d = ray-traced distance
$\mathbf{u}^g$ = unit launch vector in LGF
$\mathbf{o}^g$ = coordinates of optical centre
$\mathbf{c}^g$ = coordinates of sphere centre
r = sphere radius
∇ = discriminant for the quadratic equation

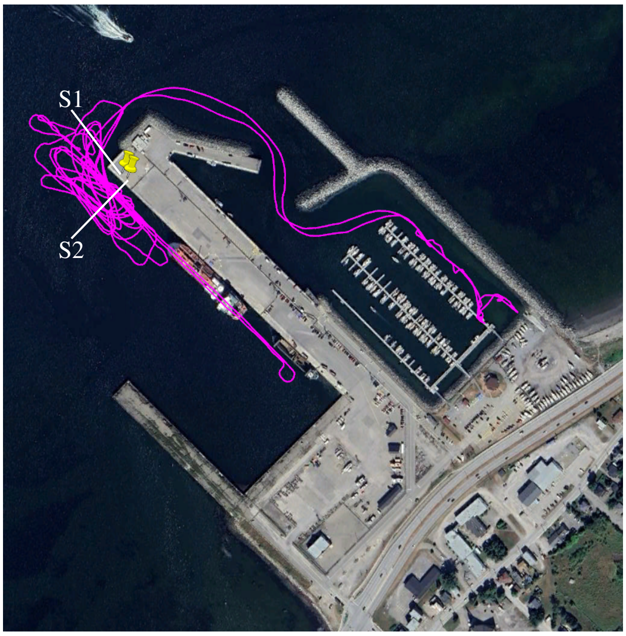

Figure 1. The trajectory used to generate synthetic data with virtual spherical targets S1 and S2 placed on the edge of the dock.

To model the scanner's range for a synthetic laser pulse we substitute equations 2 and 3 into equations 4 and 5. At this step, we control the true value for the boresight angles and the lever arm offets. We keep only the data for which there is an intersection with the spherical target and output a table that has the same format as the one produced by the VLP-16 sensor. As a result, the number of points generated was 1853 for one spherical target and 3245 for the other spherical target.

3.2 Real data production

A VLP-16 3D scanner mounted on a hydrographic vessel equipped with an Applanix POS MV is shown in figure 2. The LiDAR scanner has a 360° horizontal field of view and a 30° vertical field of view. The VLP-16 was configured to scan at 600 RPM. The Applanix navigation system has an RMS accuracy of 0.03 m in ground plane coordinates, 0.06 m in vertical coordinates as presented in the product specification. A micro geodetic survey using a total station was carried out to obtain initial estimation for the lever arm offsets.

Two spherical targets are installed on tripods at the calibration site as shown in figure 5. Their centers were surveyed using post-processed GNSS observations. The targets were then scanned in 15 different passes from various distances and directions. The scanning trajectory is shown in figure 3. A total of 6210 points were collected on the spherical targets and with more than 3000 points on each target. For each pass, the data from the spherical targets were extracted from the georeferenced clouds using a priori estimates for the boresight and and the surveyed lever arm offsets.

3.3 Calibration Algorithm

The calibration algorithm consists in finding the boresight angles and lever arm offsets that minimize the sum of positive distances from points to their corresponding sphere surface. This sum defines the objective function represented in equation 6:

Figure 2. A micro geodetic survey of a marine platform with hydrographic sensors.

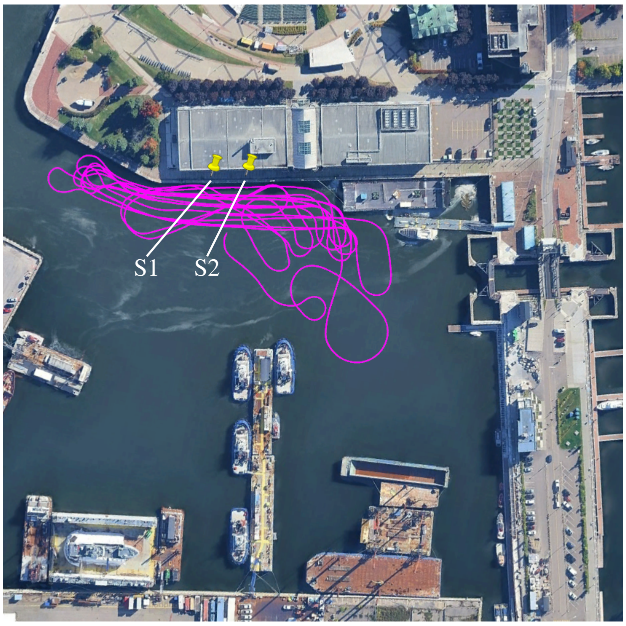

Figure 3. The trajectory used to acquire real LiDAR data with spherical targets S1 and S2 placed on the edge of the dock.

$$\arg\min_{\mathbf{b}} \sum_{j}^{N_s} \sum_{k}^{N_j} \left| \|\mathbf{x}_k(\mathbf{b}) - \mathbf{c}_j\| - r_j \right| \tag{6}$$

where N_s = number of spherical targets
N_j = number of points on jth target
$\mathbf{c}_j$ = coordinates of jth sphere centre
r = jth sphere radius
$\mathbf{x}_k$ = georeferenced point on spherical target
$\mathbf{b} = \left[\alpha, \beta, \gamma, a_x^i, a_y^i, a_z^i\right]$
(α, β, γ) = boresight alignment angles
a_x^i, a_y^i, a_z^i = lever arm offsets in INS frame i

The algorithm is based on the implementation of the Nelder-Mead simplex method (Lagarias et al., 2006) which is available in Matlab as the function fminsearch. This optimization technique does not require gradients which makes it useful for optimizing functions that are noisy, non-smooth, or difficult to differentiate. The objective function recalculates the georeferenced points on the targets using the current estimation at each iteration. The termination criteria is reached when the sum of distances to the respective sphere surfaces does not improve beyond 0.0001 m.

It is understood that this method can fail to find optimal values and become trapped in local minima. In the context of synthetic LiDAR data, a local minimum represents a set of boresight angles and lever arm offsets which fit the spherical targets but differ from the exact values used to generate the synthetic data. In the context of real LiDAR data, a local minimum would fit the spherical targets but would warp the rest of the point cloud. For this reason, we choose to place at least two spherical targets to avoid the rotation symmetry around the centre of a single spherical target. As described in the following section, we add random noise to the initial estimation of the boresight angles and the lever arm offsets in order to analyze the convergence of this objective function.

4. Results and Discussion

4.1 Calibration using synthetic data

The synthetic data is georeferenced with erroneous values for the boresight angles and lever arm offsets where we can clearly see, in Figure 4, the effects of these errors do not correspond to a translation and rotation of the point cloud. We start calibration algorithm with these erroneous value as initial estimates. Using synthetic data, the calibration algorithm converges to the true values of the boresight angles and lever arm offsets which were used to generate them. This is expected because there are no other sources of noise in this synthetic data set. We then repeat this process by adding noise to the initial estimates. For each lever arm offset the random noise is chosen between ± 0.5 m and for each boresight angle the random noise is chosen between ± 5 degrees. An automated script that runs this calibration method with this noise and logs all the intermediate data was developed. Figure 4 shows an example of a point cloud georeferenced with an erroneous set of boresight angles and lever arm offsets. It also shows the corrected point cloud georeferenced from the calibrated boresight angles and lever arm offsets. The erroneous and calibrated values used to generate these point clouds are shown in Table 1. We observe that all the points return to the surface of their respective spherical target. For every set of initial boresight angles and lever arm offsets tested by this script, the calibration algorithm converges to the true values for the boresight angles and the lever arm offsets. This suggests that the objective function defined in equation 6 has no local minima around the optimal solution.

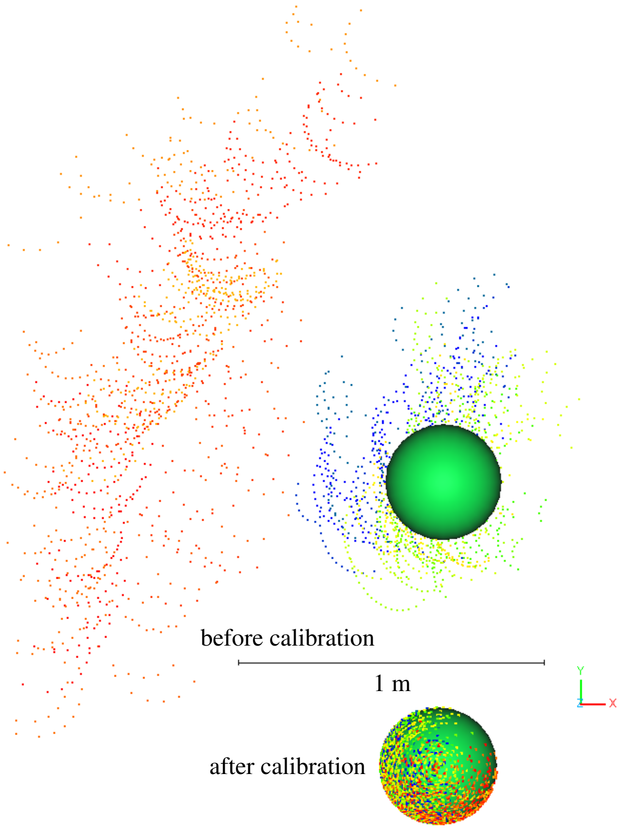

Figure 4. The georeferenced LiDAR point cloud for one spherical target before and after the calibration process using synthetic data.

Parameter	Boresight Angles (°)		
Values	Roll	Pitch	Heading
True values	179.500	-44.900	1.200
Erroneous values	181.787	-42.423	2.431
Calibrated values	179.500	-44.900	1.200
Parameter	Lever Arms (m)		
Values	X	Y	Z
True values	1.500	-1.240	-1.360
Erroneous values	1.312	-1.205	-1.759
Calibrated values	1.500	-1.240	-1.360

Table 1. Erroneous and calibrated values of boresight angles and lever arm offsets used to generate Figure 4.

4.2 Calibration using real data

First, the real LiDAR data is georeferenced using the surveyed lever arm offsets and a priori estimates for the boresight angles in order to extract the data on spherical targets. We then launch the calibration algorithm with these initial estimates and then georeference the point clouds using the resulting parameters. Figure 5 shows the point clouds limited to the target site before and after the calibration process.

Noise was added to the a priori estimation to study the sensitivity to initial conditions and existence of local minima. We chose the same noise interval as with synthetic data: $\pm 5°$ for angles and $\pm$ 0.5 m for lever arm offsets. An automated script that runs this calibration method and logs all the intermediate data was also developed. For every set of initial boresight angles and lever arm offsets tested by this script, the calibration algorithm converges to within 0.001°for the boresight angles and within 0.001 m for the lever arm offsets. Figure 6 shows an example of

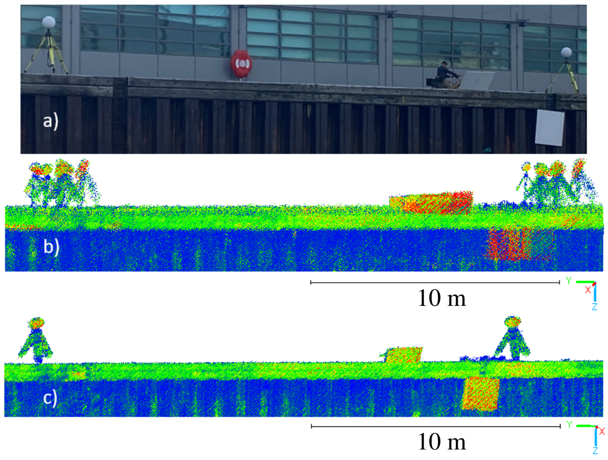

Figure 5. a) Calibration site comparing point clouds b) using initial estimates for boresight angles and lever arms and c) using their calibrated values.

a point cloud georeferenced with an erroneous set of boresight angles and lever arm offsets. It also shows the corrected point cloud georeferenced from the calibrated boresight angles and lever arm offsets. The erroneous and calibrated values used to generate these point clouds are shown in Table 2. Again, we note that the effects of these errors do not correspond to a translation and rotation of the point cloud.

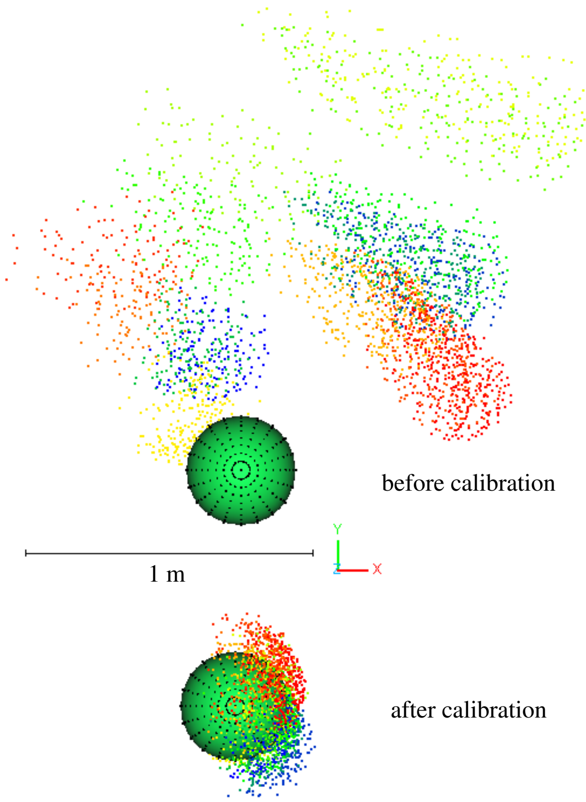

Figure 6. The georeferenced LiDAR point cloud for one spherical target before and after the calibration process using real data.

These results suggests that even in the presence of scanner and navigation system noise, the objective function defined in equation 6 has no local minima around the optimal solution and that the use of a total station may be replaced by simple tape measurements in order to obtain the initial estimates for the lever arm offsets. Figure 7 which combines all 15 point clouds acquired from the scan line pattern for the full environment shows that the alignment is maintained beyond the target site. The RMS error for the distance between the surveyed sphere centres and the fitted sphere centres is 0.036 m, which is within the range of the accuracy of the POS MV navigation system.

Parameter	Boresight Angles (°)		
Values	**Roll**	**Pitch**	**Heading**
True values	N/A	N/A	N/A
Erroneous values	-179.854	48.365	-9.737
Calibrated values	-179.732	47.579	-7.116
Parameter	**Lever Arms (m)**		
Values	**X**	**Y**	**Z**
True values	N/A	N/A	N/A
Erroneous values	0.519	-0.757	-1.653
Calibrated values	0.582	-1.223	-1.660

Table 2. Erroneous and calibrated values of boresight angles and lever arm offsets used to generate Figure 6.

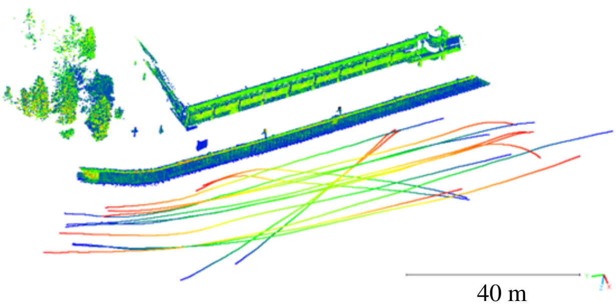

Figure 7. Superposition of 15 LiDAR scans showing a good alignment of all point clouds after the calibration process.

5. Conclusions and Future Work

This work presents a robust calibration framework for marine LiDAR systems by leveraging spherical targets to jointly estimate boresight angles and lever arm offsets. The use of spheres provides a geometrically consistent and orientation-independent reference, enabling accurate calibration even in complex marine environments. To evaluate the proposed approach, a synthetic data generation algorithm was developed to simulate LiDAR scans over spherical targets, allowing controlled testing across a wide range of sensor configurations. Finally, the calibration method was validated using real LiDAR data collected from a hydrographic survey vessel. The agreement between synthetic trials and real-world results demonstrates the effectiveness and practical applicability of the approach. The MATLAB code developed for the simultaneous estimation of a complete set of 6 LiDAR installation parameters using spherical targets is available as open-source software on GitHub (McManus, 2025).

In order to further extend the capabilities and applicability of the proposed calibration framework, the following avenues are proposed as future work. First, the implementation of an optimal line-scanning pattern and a spatial arrangement of spherical targets would improve calibration robustness and reduce field-deployment effort. A similar work with planar targets (Shahraji et al., 2020) can guide us in carrying this task. Additionally, the use of spheres as reference features offers the potential to support trajectory correction, such as SLAM, allowing navigation drift to be mitigated directly from LiDAR observations.

Furthermore, adapting this methodology for use on other multi-sensor platforms such as drones equipped with the same sensors (VLP-16 LiDAR scanner and Applanix UAV navigation system) represents a natural extension. Adapting to a different reference frame (aerial view instead of ground view), estimating an optimal height and flight pattern, and identifying the number and location of spherical targets will be essential considerations. A first experiment with a dataset acquired using a drone already demonstrates the feasibility of our approach.

Finally, to give us more flexibility in implementing the above suggested avenues of future work, we have built an in-house mobile LiDAR system composed of a Velodyne VLP-16 LiDAR scanner and a VectorNav VN-200 GNSS/IMU unit integrated in the Robot Operating System environment (Macenski et al., 2022) using the libpointmatcher SLAM algorithm (Pomerleau et al., 2013). This system is already functional as shown in Figures 8 and 9. It can be quickly mounted on various mobile platforms in order to address the challenge of obtaining LiDAR data in varying environmental conditions at low cost. It also presents a great potential for training and making LiDAR calibration methodologies more accessible.

Figure 8. In-house mobile scanning system which integrates a VLP-16 LiDAR scanner and VN200 GNSS/IMU unit.

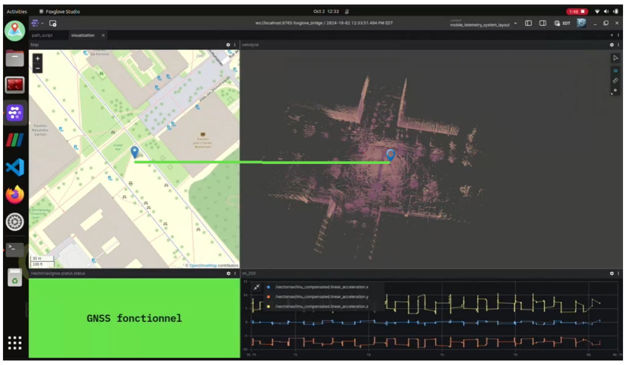

Figure 9. User interface of the in-house mobile LiDAR scanner displaying its current position and live point cloud.

6. Acknowledgement

We acknowledge the support of the Natural Sciences and Engineering Research Council of Canada (NSERC) through an Alliance Grants (ALLRP) for the project entitled “AmphibiAR research program: Development of a mobile LiDAR-SONAR system for marine infrastructure surveillance”, and our two partners in this project: Centre Interdisciplinaire de Développement en Cartographie des Océans (CIDCO) et WSP Canada Inc. We also thank Benoit Audet for the development of the in-house mobile LiDAR system and Bruno Dionne for the electronic integration of the VLP-16 scanner on WSP marine system.

References

Eberly, D., 2001. *3D Game Engine Design: A Practical Approach to Real-Time Computer Graphics*. Springer Nature.

Glira, P., Pfeifer, N., Briese, C., 2015. Automatic extrinsic self-calibration of mobile mapping systems based on geometric 3d features. *ISPRS Annals of the Photogrammetry, Remote Sensing and Spatial Information Sciences*, II-3/W4, 17–24.

González-Cancelas, N., Martínez, P., Vaca Cabrero, J., Camarero, A., 2025. Optimization of Port Asset Management Using Digital Twin and BIM/GIS in the Context of Industry 4.0: A Case Study of Spanish Ports. *Processes*, 13, 705.

Lagarias, J., Reeds, J., Wright, M., Wright, P., 2006. Convergence Properties of the Nelder–Mead Simplex Method in Low Dimensions. *SIAM Journal on Optimization*, 9, 112-147.

Liu, W., Gardoni, P., Li, Z., Krolczyk, G., Du, H., Li, W., Sotelo, M.-A., 2022. Multiple Natural Features Fusion for On-Site Calibration of LiDAR Boresight Angle Misalignment. *IEEE Transactions on Geoscience and Remote Sensing*, PP, 1-1.

Lv, J., Zuo, X., Hu, K., Xu, J., Huang, G., Liu, Y., 2022. Observability-Aware Intrinsic and Extrinsic Calibration of LiDAR-IMU Systems. *IEEE Transactions on Robotics*, 38(6), 3734–3753.

Macenski, S., Foote, T., Gerkey, B., Lalancette, C., Woodall, W., 2022. Robot Operating System 2: Design, architecture, and uses in the wild. *Science Robotics*, 7(66), eabm6074. https://www.science.org/doi/abs/10.1126/scirobotics.abm6074.

McManus, J., 2025. LiDAR raytracing and calibration developped for M.Sc. in Geomatic Sciences. `https://github.com/JordanMcManus/msc_geomatique`.

Mendez, M., 2024. A comprehensive guide to boresight and strip alignment for lidar data accuracy. Accessed: 2026-03-08.

Mishra, S., Pandey, G., Saripalli, S., 2021. Target-free extrinsic calibration of a 3d-lidar and an imu. *IEEE International Conference on Multisensor Fusion and Integration for Intelligent Systems (MFI)*, 1–7.

Pomerleau, F., Colas, F., Siegwart, R., Magnenat, S., 2013. Comparing ICP Variants on Real-World Data Sets. *Autonomous Robots*, 34(3), 133–148.

Shahraji, M., Larouche, C., 2022. Case Study: Rigorous Boresight Alignment of a Marine Mobile LiDAR System Addressing the Specific Demands of Port Infrastructure Monitoring. *Marine Geodesy*, 45, 1-18.

Shahraji, M., Larouche, C., Cocard, M., 2020. Analysis of Systematic Errors of Mobile LiDAR Systems: a Simulation Approach. *ISPRS Annals of Photogrammetry, Remote Sensing and Spatial Information Sciences*, V-1-2020, 253-260.

Zhu, F., Ren, Y., Zhang, F., 2022. Robust real-time lidar-inertial initialization. *Proceedings of the IEEE/RSJ International Conference on Intelligent Robots and Systems (IROS)*, IEEE, 3948–3955.